**Article:**
Zhao, X, Allen, RJ, Wood, T orcid.org/0000-0002-6049-5805 et al. (1 more author) (2020) Tropical belt width proportionately more sensitive to aerosols than greenhouse gases. Geophysical Research Letters, 47 (7). e2019GL086425. ISSN 0094-8276

https://doi.org/10.1029/2019GL086425

Geophysical Research Letters

RESEARCH LETTER
10.1029/2019GL086425

# Tropical Belt Width Proportionately More Sensitive to Aerosols Than Greenhouse Gases

**Xueying Zhao[1], Robert J. Allen[1], Tom Wood[2], and Amanda C. Maycock[2]**

[1]Department of Earth and Planetary Sciences, University of California, Riverside, CA, USA, [2]School of Earth and Environment, University of Leeds, Leeds, UK

**Key Points:**
- In addition to GHGs, aerosols are capable of perturbing the width of the tropics
- Increased black carbon (BC) aerosol drives tropical expansion; sulfate drives contraction
- BC, particularly from Asia, is more efficient than GHGs in driving tropical expansion, especially in the NH

**Supporting Information:**
- Supporting Information S1

**Correspondence to:**
X. Zhao,
xzhao009@ucr.edu

**Citation:**
Zhao, X., Allen, R. J., Wood, T., & Maycock, A. C. (2020). Tropical belt width proportionately more sensitive to aerosols than greenhouse gases. *Geophysical Research Letters*, *47*, e2019GL086425. https://doi.org/10.1029/2019GL086425

Received 26 NOV 2019
Accepted 15 MAR 2020
Accepted article online 18 MAR 2020

**Abstract** The tropical belt has widened during the last several decades, and both internal variability and anthropogenic forcings have contributed. Although greenhouse gases and stratospheric ozone depletion have been implicated as primary anthropogenic drivers of tropical expansion, the possible role of other drivers remains uncertain. Here, we analyze the tropical belt width response to idealized perturbations in multiple models. Our results show that absorbing black carbon (BC) aerosol drives tropical expansion, and scattering sulfate aerosol drives contraction. BC, especially from Asia, is more efficient per unit radiative forcing than greenhouse gases in driving tropical expansion, particularly in the Northern Hemisphere. Tropical belt expansion (contraction) is associated with an increase (decrease) in extratropical static stability induced by absorbing (scattering) aerosol. Although a formal attribution is difficult, scaling the normalized expansion rates to the historical time period suggests that BC is the largest driver of the Northern Hemisphere tropical widening but with relatively large uncertainty.

**Plain Language Summary** The tropical belt has widened over the past several decades, and this is associated with poleward movement of the descending branches of the Hadley Cell and the subtropical dry zones. Internal climate variability and anthropogenic forcers—including greenhouse gases and stratospheric ozone depletion—are important contributors. Leveraging idealized single-forcing experiments, we show that anthropogenic aerosols, including black carbon and sulfate, drive significant tropical expansion and contraction, respectively. Aerosols, particularly those emitted from Asia, are more efficient than greenhouse gases in perturbing tropical belt width. Although relatively large uncertainty exists, linearized scaling suggests that black carbon is the dominant driver of the Northern Hemisphere tropical widening over the historical time period.

## 1. Introduction

The width of the tropical belt is linked to the Hadley cell circulation, with strong moist air ascent in tropical deep convection zones and dry air descent in the subtropics. Tropical belt expansion over the past few decades has been observed in multiple data sets (Birner et al., 2014; Davis & Rosenlof, 2012; Hu & Fu, 2007; Lu et al., 2007; Lucas et al., 2014; Seidel et al., 2008). This expansion is indicated by several metrics, including widening of the Hadley cell (Hu & Fu, 2007; Lu et al., 2007; Nguyen et al., 2013) and poleward shifts in hydrological patterns and subtropical dry zones (Cai et al., 2012; Horinouchi et al., 2019; Scheff & Frierson, 2012; Sousa et al., 2011; Staten et al., 2018).

In addition to internal (Garfinkel et al., 2015; Grise et al., 2018) and natural (Allen & Kovilakam, 2017; Allen et al., 2014; Amaya et al., 2018; Grassi et al., 2012; Lu et al., 2008; Mantsis et al., 2017; Nguyen et al., 2013; Tandon et al., 2013) variability, anthropogenic drivers are another important contributor. Tropical widening occurs in model simulations driven by greenhouse gases (GHGs) (Grise & Polvani, 2016; Hu et al., 2013; Tao et al., 2016), which is associated with a poleward shift in the subtropical baroclinic instability zone (Lu et al., 2007). Stratospheric ozone depletion is important in the Southern Hemisphere (SH), particularly during austral summer (Min & Son, 2013; Polvani et al., 2011; Waugh et al., 2015). Absorbing aerosols, such as black carbon (BC), have been suggested as a cause of the Northern Hemisphere (NH) tropical expansion (Allen et al., 2012b, 2014; Johnson et al., 2019; Kovilakam & Mahajan, 2015; Shen & Ming, 2018). BC warms the troposphere, particularly in the NH midlatitudes where most emissions occur, which stabilizes the atmospheric column and results in a poleward shift of tropospheric jet streams (Allen et al., 2012a, 2012b;

Shen & Ming, 2018). Future decreases in scattering aerosol also induce midlatitude tropospheric warming (primarily via aerosol-cloud interactions), leading to NH tropical widening through the 21st century (Allen & Ajoku, 2016; Allen & Sherwood, 2011).

The overall impact of anthropogenic drivers on tropical belt width variations is complex and has large uncertainties. This is particularly true for aerosols, where the 90% confidence range of aerosol effective radiative forcing (ERF) is −0.4 to −2.0 W $m^{-2}$ (Bellouin et al., 2019). Similarly, BC forcing from anthropogenic fossil and biofuel emissions possesses a relatively large uncertainty range of 0.05 to 0.80 W $m^{-2}$ (Bond et al., 2013; Koch et al., 2009; Myhre et al., 2013; Ramanathan & Carmichael, 2008). The imprint of anthropogenic drivers on recent tropical expansion may even be indiscernible from natural drivers (Grise et al., 2019).

The goal of this work is to better understand the effect of anthropogenic drivers on tropical belt width variations, focused on the role of aerosols. To isolate the role of individual drivers, we utilize idealized simulations with very large single-forcing perturbations in comprehensive coupled ocean-atmosphere models from Precipitation Driver and Response Model Intercomparison Project (PDRMIP). Although the forcings are idealized and their magnitude is not realistic, they allow a direct assessment of how individual driver impacts tropical belt width (e.g., Davis et al., 2016). This is the first study that rigorously quantifies the aerosol impact—including individual aerosol species like BC and sulfate—on tropical belt width using multiple models. Moreover, this is the first study that quantifies the impact of regional (e.g., Europe, Asia) aerosol emissions on tropical belt width. Methods and data are described in section 2. Section 3 discusses the results, and section 4 summarizes our conclusions.

## 2. Method and Data

### 2.1. Model Simulations

Under the framework of PDRMIP (Myhre et al., 2017), we use the coupled global model simulations including the baseline simulation and a set of perturbation experiments. The baseline simulation is forced with all anthropogenic and natural climate forcing agents at present-day (year 2000) levels (Samset et al., 2016). Global perturbation experiments (relative to present day)—which represent very large perturbations, particularly for the aerosols—include a doubling of carbon dioxide (co2×2), 10 times BC concentration or emissions (bc×10), and 5 times sulfate concentrations or emissions (sul×5). Regional aerosol perturbation experiments include 10 times Asian BC concentration or emissions (bc×10 Asia) and 10 times sulfate concentrations or emissions in Europe (sul× 10 EU) and Asia (sul× 10 Asia) (Liu et al., 2018). The European (Asian) region is defined from 35°N to 70°N and 10°W to 40°E (10°N to 50°N and 60°E to 140°E). An exception is HadGEM2-ES, which uses emissions from the year 1860 for its base run, and perturbation simulations are relative to the year 2000 (Stjern et al., 2017). HadGEM2-ES simulations will therefore feature larger increases in aerosols.

Nine models are used for the global perturbation experiments including CanESM2, HadGEM2-ES, HadGEM3, GISS-E2-R, MIROC-SPRINTARS, NCAR CESM1-CAM4, NCAR CESM1-CAM5, IPSL-CM5A, and NorESM1 (Myhre et al., 2017; Samset et al., 2016). All models use a fully dynamical ocean model, except NCAR CESM1-CAM4 which uses a slab ocean model. Most models also performed regional perturbation experiments, except CanESM2 and HadGEM2. Although some models are concentration driven and some are emission driven, we do not find clear response differences between emission- and concentration-driven models. All simulations are interpolated to a 2.5° by 2.5° grid resolution using bilinear interpolation. We analyze the last 50 years of each simulation, when near-equilibrium is reached. For most experiments, models do not show significant trends in net top-of-atmosphere radiative fluxes over the last 50 years. However, in the case of co2×2, models will likely not have reached their equilibrium warming within the 100 years simulated here (Caldeira & Myhrvold, 2013; Samset et al., 2016).

We also use the corresponding PDRMIP fixed sea surface temperature (fSST) experiments to estimate the ERF, as well as the fast response (no surface temperature feedbacks) of the tropical belt width. ERF is estimated from the net top-of-atmosphere radiative fluxes (the sum of net longwave and shortwave fluxes) from the fSST simulations (perturbation minus baseline). This ERF definition is similar to Forster et al. (2016), except SSTs here are based on the baseline climatology as opposed to the preindustrial. All fSST simulations were performed for at least 15 years, so we analyze the last 15 years of data for these calculations. The 90% confidence interval for a 15 year aerosol ERF is ∼0.15 W $m^{-2}$ (Forster et al., 2016). Annual global and hemispheric mean ERFs for individual models and experiments are included in supporting information Tables

S1 and S2, and spatial ERF maps are including in supporting information Figure S1. As the coupled simulations yield the total climate response (slow surface temperature feedbacks and fast rapid adjustments), the fSST simulations yield the fast response (e.g., atmospheric heating).

### 2.2. Tropical Edge Definition

The Tropical-width Diagnostics package (Adam et al., 2018) is used to calculate the location of the tropical belt edge. The Tropical-width Diagnostics package includes common tropical width metrics and standardizes the methodologies to diagnose the tropical belt edge by implementing simple mathematical methods. As recommended by Davis and Birner (2017) and Waugh et al. (2018), we focus on three metrics of tropical width: (1) the latitude where the zonal mean meridional circulation (MMC) at 500 hPa becomes zero on the poleward side of the subtropical maxima, (2) the zero-crossing latitude where the zonal mean near-surface easterly becomes midlatitude westerly at the poleward side of the subtropical minimum in each hemisphere and equatorward of 60° latitude (UAS), and (3) the latitude where the zonal mean precipitation minus evaporation becomes zero on the poleward side of the subtropical minimum (P-E). Changes in the latitude of the tropical belt edge are calculated as the difference between the perturbation simulation and the corresponding baseline simulation. Positive (negative) anomalies indicate tropical expansion (contraction). Note that GISS-E2-R did not archive output to calculate the MMC metric. We have verified that similar results are obtained in the other two metrics when GISS-E2-R is removed from the the multimodel mean (not shown). We also note that recent analyses have generalized the MMC to the regional level by using the horizontally divergent wind (Schwendike et al., 2014; Staten et al., 2019). For conciseness, the quoted rates of expansion in the text are based on the average across the three metrics. In general, we get very similar results for all three metrics, but where exceptions exist, they are noted. The figures show all metrics separately.

Statistical significance of tropical belt changes is examined by a standard two-tail $t$ test, accounting for the influence of serial correlation by using the effective sample size, $nyears(1 - r_1)(1 + r_1)^{-1}$, where $nyears$ is the number of years and $r_1$ is the lag-1 autocorrelation coefficient. The 90% confidence interval of ensemble mean response is also quantified as twice the standard error, $2 \times \sigma/\sqrt{n}$, where $\sigma$ is the intermodel standard deviation of the tropical width changes and $n$ is the number of models. We also quantify tropical width variations due to internal climate variability as the 90% confidence interval of tropical edge locations from the baseline simulation for each model. This is calculated by quantifying the boundary of the tropical edge in each hemisphere for each season and the annual mean for all years ($nyears$). The 90% confidence interval is based on a $t$ test and estimated according to $\bar{\Phi} \pm 1.68 \times \frac{\sigma'}{\sqrt{nyears}}$, where $\sigma'$ is the standard deviation of tropical edge locations, $nyears$ is the number of tropical edge locations (i.e., number of years), $\bar{\Phi}$ is the mean tropical belt edge location, and 1.68 is the $t$ value with $nyears$-1 (49 for the coupled runs) degrees of freedom and a 0.05 probability.

Supporting information Figure S2 shows individual model confidence intervals; the multimodel mean confidence interval ranges from 0.18° for MMC to 0.22° for P-E in the NH and from 0.08° for MMC to 0.11° for UAS in the SH. The smaller values in the SH may be due to the more zonally symmetric circulation and lack of land-sea contrasts. It may also be an artifact of finding the edge of the tropical belt, which is less well defined in the NH (Adam et al., 2018)—especially for June-July-August (JJA)—which would also lead to enhanced variability in the NH.

## 3. Results

The annual mean tropical belt edge response to anthropogenic drivers in the global perturbation experiments is shown in Figure 1. Consistent with prior studies (Grise & Polvani, 2016; Tao et al., 2016), co2×2 leads to tropical expansion. However, we find relatively weak tropical expansion in the NH and much stronger and significant expansion in the SH. The annual mean ensemble mean poleward displacement of the SH tropical edge (~1° ± 0.19°) is about 5 times that of NH (~0.2° ± 0.15°). Watt-Meyer et al. (2019) found twice as much GHG-induced tropical expansion in the SH, relative to the NH. GHG-forced tropical expansion is significant relative to internal climate variability in the SH but not in the NH (gray shading in Figure 1). The weaker rate of annual mean widening in the NH is partly due to tropical contraction during JJA in all metrics (supporting information Figures S3–S5). This result is consistent with prior analyses, where CMIP5 historical GHG and co2×4 simulations also yield NH tropical contraction during JJA (Grise & Polvani, 2016; Tao et al., 2016; Watt-Meyer et al., 2019). Further analysis is warranted, but this may be related to the JJA

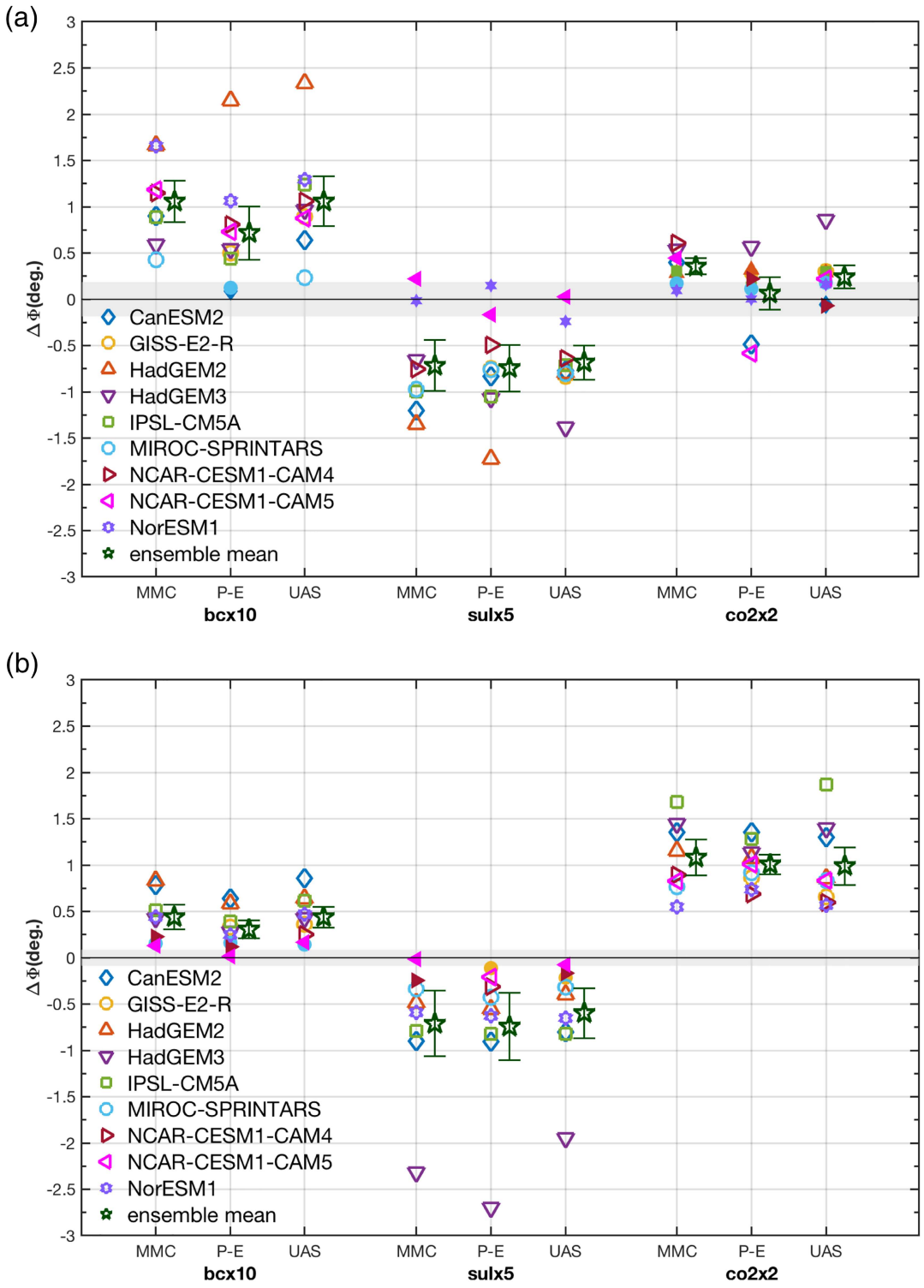


**Figure 1.** Annual mean tropical belt edge response in global perturbation experiments. (a) Northern Hemisphere and (b) Southern Hemisphere tropical belt edge change (° latitude) in response to bc×10, sul×5, and co2×2 based on the MMC, P-E, and UAS metric for each individual model. Positive (negative) anomalies indicate tropical expansion (contraction). Unfilled model symbols indicate a response statistically significant at the 90% confidence level. The corresponding ensemble mean response is denoted by a dark green star, and the error bar shows the approximate 90% confidence interval, estimated by $2 \times \sigma/\sqrt{n}$, where $\sigma$ is the intermodel standard deviation of the tropical width changes, and $n$ is the number of models. Gray shading shows the 90% confidence interval of tropical belt edge displacements due to internal climate variability based on MMC metric (the 90% confidence intervals from the other two metrics are similar).

stationary wave response to $CO_2$ (Shaw, 2014; Shaw & Voigt, 2015). The largest NH widening trend due to co2×2 occurs in September-October-November (SON) (Davis et al., 2016; Grise & Polvani, 2016).

Similar to the single-model result from Kovilakam and Mahajan (2015), the bc×10 simulation yields significant tropical expansion in both hemispheres across all three metrics. The magnitude of annual mean ensemble mean NH tropical expansion (~0.96° ± 0.12°) is 2.3 times larger than in the SH (~0.41° ± 0.12°). This NH amplification is in contrast to co2×2 (where NH expansion is 20% as large as that in the SH), which is likely related to more BC burden in the NH and consequently a larger hemispheric asymmetry in BC forcing (supporting information Table S1 and Figure S1). HadGEM2-ES generally yields the largest tropical expansion, especially in the NH, which is consistent with its large change in burden (Stjern et al., 2017) and relatively large BC ERF (supporting information Table S1). All seasons also show robust tropical expansion in response to bc×10 in both hemispheres (supporting information Figures S3–S5), with maximum tropical widening occurring in the NH during JJA and SON and in the SH during December-January-February and SON. The large JJA BC response is interesting in light of the minimal JJA co2×2 expansion, which mainly results from the NH contraction in that season.

In contrast to BC, sul×5 drives significant annual mean tropical contraction in both hemispheres, at ~0.69° ± 0.24° for the NH and ~0.66° ± 0.33° for the SH. HadGEM3 yields the strongest tropical contraction, especially in the SH, consistent with its large sul×5 ERF (supporting information Table S1). Significant contraction also occurs in all seasons in both hemispheres except for JJA in the NH. Similar seasonal rates of contraction exist in the SH, while relatively large seasonal variations exist in the NH, with maximum contraction in SON. The absence of NH contraction in JJA and the strongest contraction occurring in SON are analogous but opposite to the response to co2×2.

In terms of the regional perturbation simulations, bc×10 Asia yields significant tropical expansion (Figure 2). In the NH, the annual mean ensemble mean NH tropical expansion is ~0.36° ± 0.12°. We note that the P-E metric yields about half of the NH expansion (0.20°) as the other two metrics (0.45–0.48°). Despite bc×10 Asia's global (NH) ERF being only 15% (25%) of the corresponding ERF in bc×10, bc×10 Asia's NH tropical expansion is about 40% of the corresponding expansion in bc×10. This results suggests the importance of the forcing location, with Asian BC particularly efficient at widening the tropical belt. Maximum NH tropical expansion occurs in JJA (supporting information Figures S6–S8). Significant tropical expansion also occurs in the SH, but it is much weaker at ~0.05° ± 0.04° (and within the 90% confidence interval due to internal climate variability).

The sul×10 Asia simulations yield significant NH contraction at ~0.41° ± 0.18°, with maximum NH contraction in SON. Despite sul×10 Asia's global (NH) ERF being only 21% (32%) of the corresponding ERF in sul×5, sulx10 Asia's NH annual tropical contraction is 60% of the corresponding contraction in sulx5. This result again supports the importance of the location of the forcing to tropical width perturbations. The SH tropical belt edge response to Asian sulfate is not robust and is inconsistent across metrics and seasons. The effect of European sulfate on tropical belt variations is also negligible and not significantly different from internal climate variability. sul×10 Europe accounts for 9% (15%) of the sul×5 global (NH) ERF and 10% of the NH tropical contraction. So unlike the Asian region, the tropical belt is not particularly sensitive to European sulfate emissions. As minimal NH contraction occurs under European sulfate, this implies the importance of sulfate from other regions (e.g., Asia and perhaps the United States). For SH contraction, the importance of sulfate from regions other than Europe and Asia is also implied from the large sul×5 SH contraction but minimal contraction under sul×10 Asia and sul×10 EU.

All global (and regional) aerosol experiments show larger annual mean ensemble mean tropical edge displacements in the NH, as compared to the SH (particularly bc×10). This is related to the spatial heterogeneity of aerosols, with maximum loading and more importantly, ERF in the NH. For example, the annual mean ensemble mean bc×10 ERF is 1.59 W $m^{-2}$ in the NH, compared to 0.38 W $m^{-2}$ in the SH. By design, the regional aerosol experiments also have a much larger NH ERF, relative to the SH. However, for $CO_2$ forcing—which is uniform between hemispheres—much smaller tropical widening occurs in the NH. Watt-Meyer et al. (2019) ascribe this hemispheric asymmetry in $CO_2$ tropical expansion to a smaller sensitivity of the NH tropical edge to static stability changes. Of lesser importance is the pattern of the SST response and the $CO_2$ direct radiative effect.

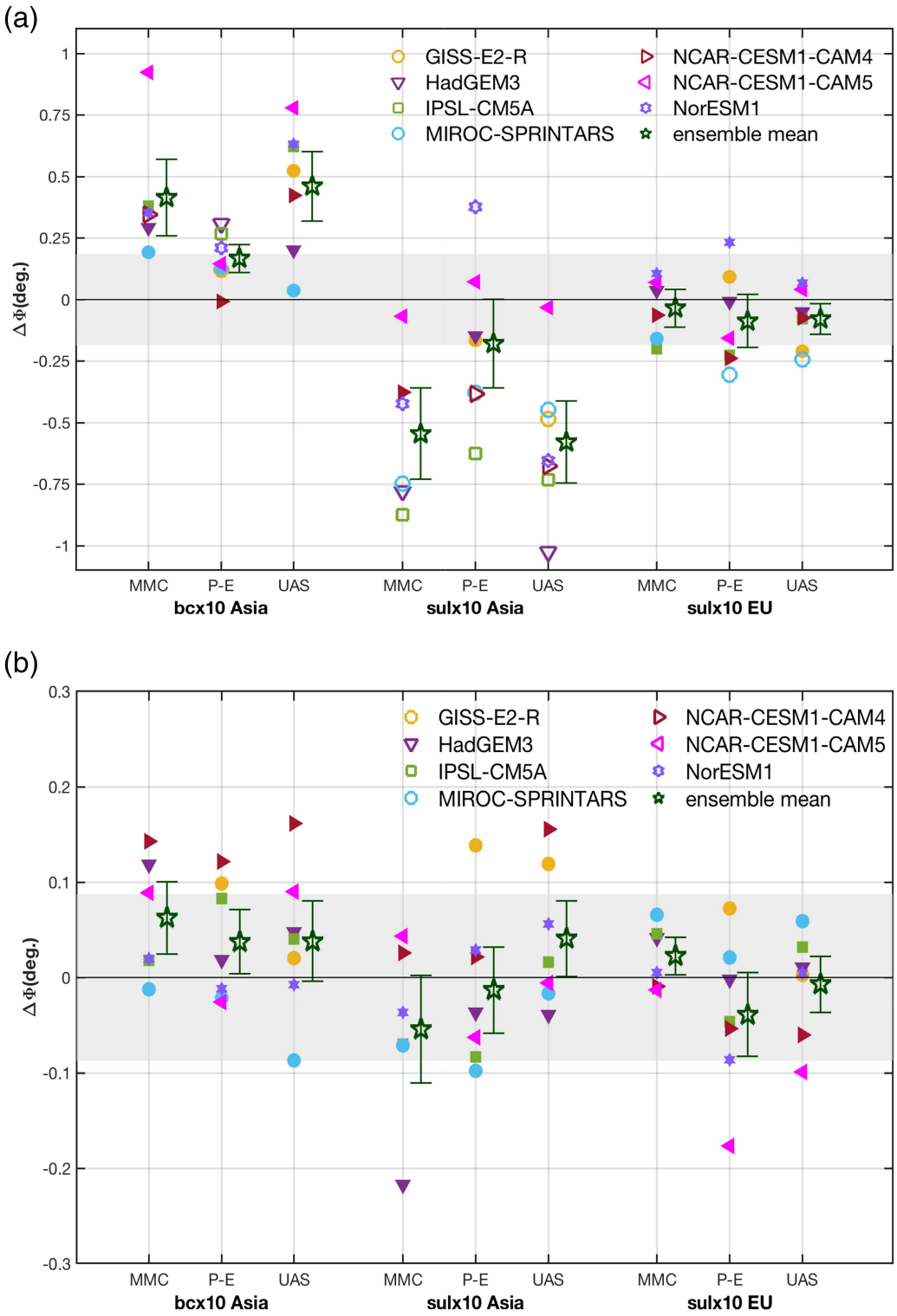


**Figure 2.** As in Figure 1 except for regional aerosol simulations including bc×10 Asia, sul×10 Asia, and sul×10 EU. Note the different *y* axis between the two panels.

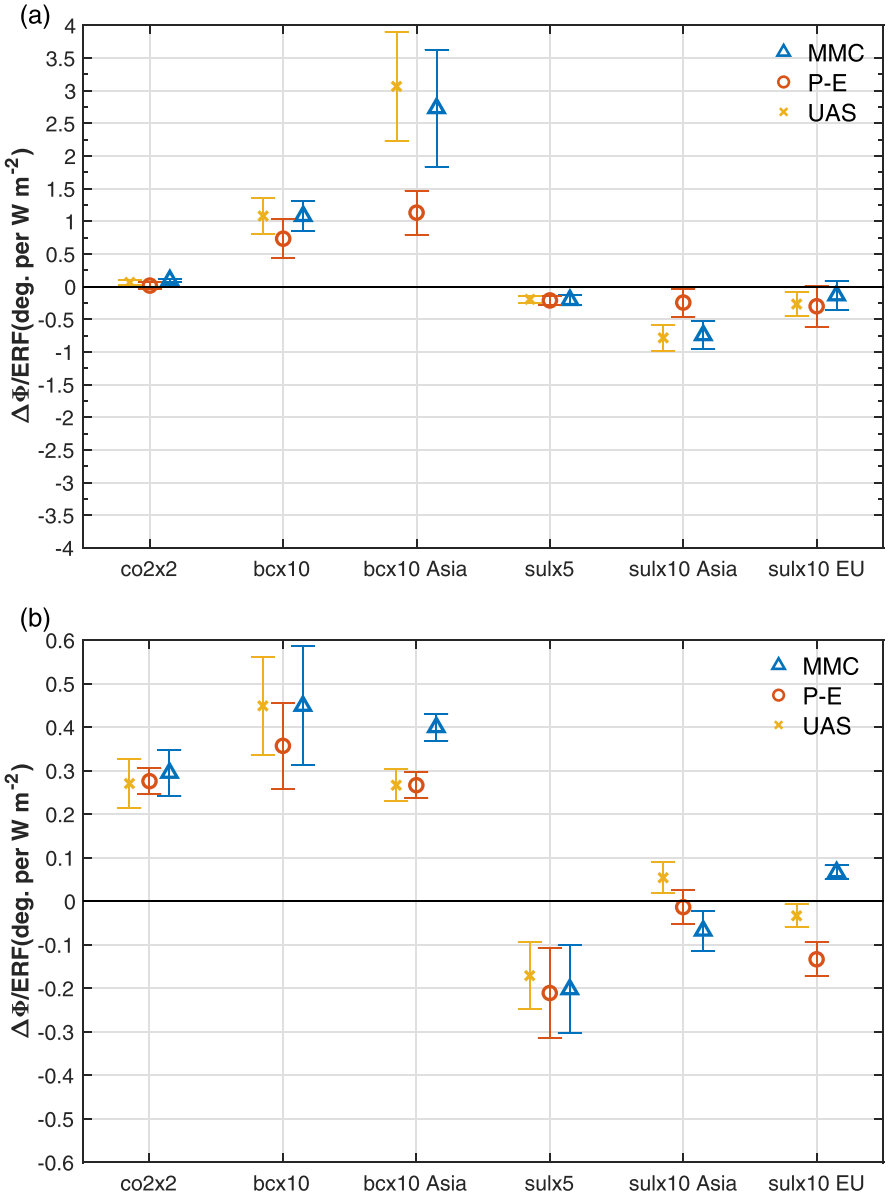


**Figure 3.** Efficacy of anthropogenic drivers in perturbing the tropical belt edge. (a) Northern Hemisphere and (b) Southern Hemisphere annual mean ensemble mean normalized tropical belt edge response to co2×2, bc×10, bc×10 Asia, sul×5, sul×10 Asia, and sul×10 EU based on the MMC, P-E, and UAS metric. The tropical belt edge response is normalized by the absolute value of the corresponding effective radiative forcing (ERF). Units are degree latitude per W $m^{-2}$. A positive (negative) response indicates tropical expansion (contraction). Note the different $y$ axes between the two panels. The 90% confidence interval is also included, estimated as $2 \times \sigma/\sqrt{n}$, where $\sigma$ is the intermodel standard deviation of the normalized tropical width changes, and $n$ is the number of models.

The seasonal cycle of the NH and SH tropical edge response does not appear to be related to the seasonal cycle of global or hemispheric ERF. For example, bc×10 NH ERF is weakest in SON at 1.04 W $m^{-2}$ when NH tropical expansion is relatively large (supporting information Figures S3–S5). Similarly, bc×10 NH ERF is largest in March-April-May (MAM) at 2.38 W $m^{-2}$ when NH tropical expansion is relatively weak. We also note that latitudinal variations in the seasonal ERF are relatively small and likely not an important contributor to the seasonal cycle of tropical edge displacements (not shown). These results reinforce the notion that there are certain seasons in which the tropical edge is more susceptible to latitudinal displacements (Grise et al., 2018; Watt-Meyer et al., 2019).

Since each of the PDRMIP idealized experiments has a different forcing magnitude, to better compare the role of aerosols versus GHGs on tropical belt width, we normalize the ensemble mean tropical belt response by the corresponding global ERF. In the case of the sulfate experiments, which have a negative ERF, we take the absolute value of the ERF so that expansion (contraction) is still represented by positive (negative) values. Figure 3 shows the ensemble mean annual mean ERF normalized tropical belt response to anthropogenic drivers. Aerosols generally drive larger NH tropical belt responses per ERF relative to GHGs. The NH tropical belt is most sensitive to BC (0.96° per W $m^{-2}$), and in particular Asian BC (2.32° per W $m^{-2}$). Again, the quoted rates of tropical expansion represent the average over the three metrics. We note that the P-E metric for bc×10 Asia yields a relatively small rate of expansion at 1.06° per W $m^{-2}$, versus ∼3° per W $m^{-2}$ for the other two metrics. Compared to BC, the sensitivity of the NH tropical edge to sulfate is weaker. However, Asian emissions again yield the largest response (−0.55° per W $m^{-2}$) among the sulfate experiments. GHGs yield a much smaller normalized rate of NH tropical expansion at ∼0.06° per W $m^{-2}$.

In the SH, anthropogenic aerosols generally show smaller efficacy in driving tropical edge perturbations as compared to the NH. Global BC yields the largest SH efficacy at ∼0.41° per W $m^{-2}$, followed by Asian BC. Global sulfate yields a SH efficacy of −0.19° per W $m^{-2}$. In contrast to the aerosols, GHGs are more effective in perturbing the SH tropical edge (0.27° per W $m^{-2}$), as compared to the NH. Although not statistically significant, global BC and to some extent Asian BC still yield larger SH efficacies than co2×2. This suggests that tropical width perturbations may be more responsive to the direct atmospheric heating by BC, as opposed to surface temperature-driven feedbacks by $CO_2$ and $SO_4$. For both hemispheres, similar conclusions exist when we normalize by the change in global mean surface temperature, as opposed to ERF (supporting information Figure S9).

The larger displacement of the tropical belt edge in response to global aerosols, particularly BC, relative to GHGs suggests the potential importance of aerosols in perturbing the tropical belt, especially in the NH. Compared to global BC and sulfate forcing, the relatively large NH response to the corresponding Asian aerosol indicates that the location of the aerosol forcing is important. This is also supported by the larger NH tropical belt contraction in response to Asian sulfate, relative to European sulfate. These results imply that a forcing closer to the tropical belt edge is likely more effective in driving changes to tropical belt width, which is generally consistent with previous idealized simulations (Allen et al., 2012a).

Under one view, the width of the Hadley cell is determined by the poleward extent to which the angular momentum conservation continues until the resulting vertical shear becomes baroclinically unstable (Lu et al., 2007). Under such a scaling, the edge of the Hadley cell is sensitive to the gross static stability and the tropopause height near the poleward boundary of the circulation. Although this scaling is instructive, in reality, the flow does not always conserve angular momentum (Schneider, 2006). We calculate the annual mean midlatitude static stability, $S$, as the potential temperature difference between the tropopause and surface ($\theta_{TP}$-$\theta_{SFC}$), averaged over 30°–60° latitude, and the response (perturbation minus baseline) is normalized by the corresponding global ERF (absolute value in the case of sulfate). We estimate $S$ from zonal mean temperature, as opposed to grid box by grid box values. Similar results are obtained when $S$ is calculated over 30°–60°, as well as from 20°–40° and 30°–40° latitude.

The ensemble mean global ERF normalized tropical belt response is well correlated with the corresponding normalized midlatitude $\Delta S$ (Figure 4). In the NH, correlations range from 0.97 to 0.98, depending on the metric. In the SH, the corresponding correlations range from 0.94 to 0.98. Similar but somewhat weaker correlations are obtained without normalizing. Normalizing by the change in global mean surface temperature (as opposed to ERF) yields analogous conclusions (supporting information Figure S10). Comparing $\Delta\Phi$ versus $\Delta$TAS (as opposed to $\Delta S$) yields similar correlations in the SH but somewhat weaker correlations in the NH (supporting information Figure S11). Figure 4 shows that GHGs and absorbing aerosols drive an increase in the midlatitude static stability, whereas scattering aerosols yield a decrease. The larger aerosol-induced tropical belt response in the NH, relative to the SH, is consistent with larger perturbations to the NH extratropical static stability. Asian aerosols also lead to larger increases in the NH midlatitude static stability, relative to the corresponding global forcing and GHGs. This supports our previous assertion that the location of the aerosol forcing is an important factor in the tropical belt width response. The $\Delta\Phi$ versus $\Delta S$ global ERF normalized correlations across model experiments—particularly for the annual mean—are also quite significant and also generally larger than global ERF normalized $\Delta\Phi$ versus $\Delta$TAS (supporting information Tables S4–S6).

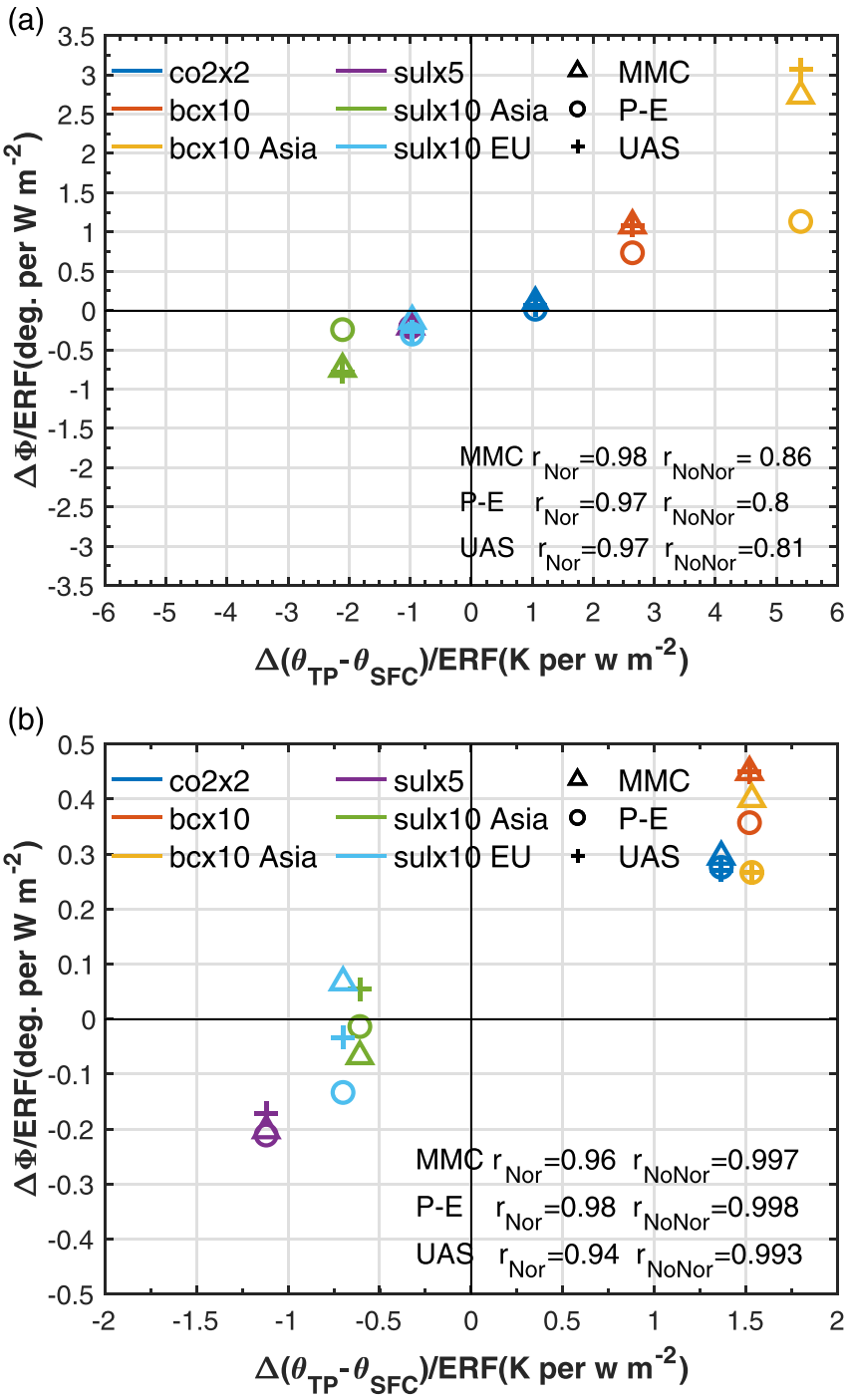


**Figure 4.** Efficacy of tropical width perturbations versus normalized extratropical static stability. Scatterplot of the annual mean ensemble mean (a) Northern Hemisphere and (b) Southern Hemisphere tropical belt edge response versus the corresponding subtropical static stability response. Both are normalized by the absolute value of the corresponding effective radiative forcing (ERF). The tropical belt edge response is based on the MMC, P-E, and UAS metric, as represented by the different symbols. A positive (negative) tropical belt edge response indicates tropical expansion (contraction). Also included are the correlations of normalized ($r_{Nor}$) and unnormalized ($r_{NoNor}$) tropical belt edge and extratropical static stability. Note the different *x* axes and *y* axes between the two panels.

Across drivers, $\Delta S$ come from different mechanisms. For $CO_2$ and sulfate, surface-driven feedbacks are most important, whereas for BC atmospheric absorption is also important. For the global forcing experiments, the fast $\Delta S$ (from the fSST experiments) is a larger proportion of the total $\Delta S$ (from the coupled experiments) in bc×10, as compared to sul×5 and co2×2 (supporting information Figure S12 and Table S3). Based on 30–60°N (global), the fast $\Delta S$ in bc×10 is 30% (15%) of the total $\Delta S$; in co2×2, the fast $\Delta S$ is 9% (7%) of the total $\Delta S$, and in sul×5 the fast $\Delta S$ is 14% (6%) of the total $\Delta S$. Thus, the fast response (i.e., direct atmospheric heating) is about 2–3 times more important in the global BC simulation, relative to the global $CO_2$ and $SO_4$ simulations. Similar results are found for the regional forcing experiments. Based on 30–60°N (global), the fast $\Delta S$ in bc×10 Asia is 81% (69%) of the total $\Delta S$; in sul×10 Asia, the fast $\Delta S$ is 33% (19%) of the total $\Delta S$. Although it is difficult to separate $\Delta S$ from $\Delta$TAS (supporting information section S1), these results suggest that direct atmospheric heating by BC drives a large fraction of the $\Delta S$.

We also calculate changes in tropical belt width from the fSST experiments. Although fewer significant responses occur, conclusions similar to those from the coupled simulations generally exist, including tropical expansion (contraction) under BC ($SO_4$)—particularly with Asian emissions—and weak NH tropical expansion under $CO_2$ (supporting information Figures S13 and S14). For the global simulations, we find that bc×10 fSST widening is a larger proportion of the total widening as compared to co2×2 and sul×5, especially in the NH (supporting information Table S3). bc×10 fSST widening is 52% and 54% of the total widening in the NH and SH, respectively. For co2×2 (sul×5) the corresponding percentages are 5% and 22% (15% and 21%). Similar results also exist for the regional experiments, particularly in the NH (where the signal is significant) for bc×10 Asia versus sul×10 Asia. The larger proportion of tropical widening in the fSST runs is consistent with the larger proportion of $\Delta S$ in the fSST runs for BC. This, in turn, supports the role of $\Delta S$ in BC-induced tropical widening and the role of direct atmospheric heating.

As previously mentioned, Watt-Meyer et al. (2019) argue that the hemispheric contrast in GHG-induced tropical expansion is related to weaker sensitivity to static stability changes in the NH. For nonnormalized annual mean tropical edge displacements and $\Delta S$ across experiments, the ensemble mean MMC-based tropical width sensitivity to $\Delta S$ is 0.19° $K^{-1}$ with a model range of 0.07–0.29° $K^{-1}$ in the NH. In the SH, the MMC-based tropical width sensitivity to $\Delta S$ is 0.19 (0.07–0.24)° $K^{-1}$. Thus, we obtain a similar tropical width sensitivity to $\Delta S$ in both hemispheres. Similar conclusions generally exist with other metrics and seasons. However, across models, $CO_2$ does yield weaker NH sensitivity (supporting information Tables S7–S9).

## 4. Conclusions

It is difficult to use the PDRMIP idealized simulations to attribute the observed tropical belt expansion to anthropogenic forcings, particularly in the case of aerosols, which have changed spatially and temporally over recent decades (Hoesly et al., 2018). Owing to the step change perturbations, PDRMIP integrations may be expected to yield a larger response relative (per unit forcing) to the real-world situation, since the system has had more time to equilibrate. Natural variability must also be considered, as it likely has played a crucial role in recent tropical expansion, while also disguising the fingerprint of anthropogenic forcing (Staten et al., 2018). Nonetheless, to illustrate the impact of these drivers on tropical widening in response to real-world changes in emissions, we follow Tang et al. (2018) and approximate the impact of GHGs, BC, and sulfate on tropical belt width by scaling the tropical belt response for each individual forcing and hemisphere according to $\Delta\Phi_{scaled} = \Delta\Phi \times (ERF_{1750-2011}/ERF_{PDRMIP})$. We use a 1750–2011 GHG forcing of 2.83 W $m^{-2}$ (90% confidence range of 2.54–3.12 W $m^{-2}$), a BC forcing of 0.40 W $m^{-2}$ (0.05 to 0.80 W $m^{-2}$), and a sulfate forcing of −0.40 W $m^{-2}$ (−0.60 to −0.20 W $m^{-2}$) (Myhre et al., 2013). Including aerosol-cloud interactions likely doubles the sulfate forcing (multimodel mean total sulfate forcing of −0.89 W $m^{-2}$ with a range from −0.34 to −1.62 W $m^{-2}$) (Boucher et al., 2013). Furthermore, BC thermodynamic effects on clouds are not accounted for here (e.g., Allen et al., 2019). Using these forcings and the ERF normalized tropical edge response for each driver and hemisphere (and assuming linearity to ERF), we estimate 1750–2011 NH tropical widening of 0.17° (0.15° to 0.19°) for GHGs, 0.38° (0.05° to 0.77°) for BC, and −0.1° (−0.15° to −0.05°) for sulfate. In the SH, we estimate 0.76° (0.69° to 0.84°) for GHGs, 0.16° (0.02° to 0.33°) for BC, and −0.08° (−0.11° to −0.04°) for sulfate. Cross checking the GHG results with CMIP5 GHG-only tropical widening trends over a similar (but somewhat different) time period of 1850–2005 yields tropical widening of 0.23° in the NH and 0.70° in the SH (Allen & Ajoku, 2016). These values compare well to the above GHG inferred estimates. Although this approach represents an approximation and possesses several caveats, it suggests that among the drivers, BC has likely caused a substantial portion NH tropical widening over the historical time period.

However, we reiterate the large uncertainty associated with BC forcing, with a 90% confidence range of 0.05 to 0.80 W $m^{-2}$ (Bond et al., 2013; Koch et al., 2009; Myhre et al., 2013; Ramanathan & Carmichael, 2008). To the extent that BC and sulfate (or other reflecting aerosols) are coemitted, however, this will partially offset the BC effect, especially when aerosol-cloud radiative effects are accounted for. Even so, the net effect of BC and sulfate on the NH tropical edge is similar to GHGs at 0.18° and 0.17°, respectively.

Our results are able to isolate and highlight the role of aerosols, particularly from Asia, in perturbing the width of the tropical belt. Given large anticipated reductions in aerosol emissions over the next few decades (Rao et al., 2017), including emissions from Asia, our results imply a possibly large role of aerosols in future perturbations to the width of the tropical belt. Future studies should focus on more realistic, time-varying aerosol simulations where the regional and seasonal features of aerosol-induced tropical belt variations can be analyzed. Moreover, given the large amplitude of the perturbations considered here, a large ensemble of such simulations is likely necessary to detect any anthropogenic aerosol signal, relative to natural variability.

**Acknowledgments**
The authors declare no competing financial interests. PDRMIP simulations can be accessed online (https://cicero.oslo.no/en/PDRMIP/PDRMIP-data-access/). We thank Apostolos Voulgarakis, Jean-François Lamarque, Olivier Boucher, Duncan Watson-Parris, and Bjørn Samset for helpful comments on an initial draft. We thank two anonymous reviewers for helpful comments and time devoted to evaluating our manuscript.

## References

Adam, O., Grise, K. M., Staten, P., Simpson, I. R., Davis, S. M., Davis, N. A., et al. (2018). The TropD software package (v1): Standardized methods for calculating tropical-width diagnostics. *Geoscientific Model Development*, *11*(10), 4339–4357.

Allen, R. J., & Ajoku, O. (2016). Future aerosol reductions and widening of the northern tropical belt. *Journal of Geophysical Research: Atmospheres*, *121*, 6765–6786. https://doi.org/10.1002/2016JD024803

Allen, R. J., Amiri-Farahani, A., Lamarque, J.-F., Smith, C., Shindell, D., Hassan, T., & Chung, C. E. (2019). Observationally constrained aerosol-cloud semi-direct effects. *npj Climate and Atmospheric Science*, *2*(1), 1–12. https://doi.org/10.1038/s41612-019-0073-9

Allen, R. J., & Kovilakam, M. (2017). The role of natural climate variability in recent tropical expansion. *Journal of Climate*, *30*(16), 6329–6350.

Allen, R. J., Norris, J. R., & Kovilakam, M. (2014). Influence of anthropogenic aerosols and the Pacific Decadal Oscillation on tropical belt width. *Nature Geoscience*, *7*(4), 270–274.

Allen, R. J., & Sherwood, S. C. (2011). The impact of natural versus anthropogenic aerosols on atmospheric circulation in the community atmosphere model. *Climate Dynamics*, *36*(9-10), 1959–1978.

Allen, R. J., Sherwood, S. C., Norris, J. R., & Zender, C. S. (2012a). The equilibrium response to idealized thermal forcings in a comprehensive GCM: Implications for recent tropical expansion. *Atmospheric Chemistry and Physics*, *12*(10), 4795–4816.

Allen, R. J., Sherwood, S. C., Norris, J. R., & Zender, C. S. (2012b). Recent Northern Hemisphere tropical expansion primarily driven by black carbon and tropospheric ozone. *Nature*, *485*(7398), 350–354.

Amaya, D. J., Siler, N., Xie, S.-P., & Miller, A. J. (2018). The interplay of internal and forced modes of Hadley cell expansion: Lessons from the global warming hiatus. *Climate Dynamics*, *51*(1-2), 305–319.

Bellouin, N., Quaas, J., Gryspeerdt, E., Kinne, S., Stier, P., Watson-Parris, D., et al. (2019). Bounding global aerosol radiative forcing of climate change. *Reviews of Geophysics*, *57*, e2019RG000660. https://doi.org/10.1029/2019RG000660

Birner, T., Davis, S., & Seidel, D. (2014). Earth's tropical belt. *Physics Today*, *67*(12), 38–44.

Bond, T. C., Doherty, S. J., Fahey, D. W., Forster, P. M., Berntsen, T., DeAngelo, B. J., et al. (2013). Bounding the role of black carbon in the climate system: A scientific assessment. *Journal of Geophysical Research: Atmospheres*, *118*, 5380–5552. https://doi.org/10.1002/jgrd.50171

Boucher, O., Randall, D., Artaxo, P., Bretherton, C., Feingold, G., Forster, P., et al. (2013). Clouds and aerosols. In T. F. Stocker, et al. (Eds.), *Climate change 2013: The physical science basis. Contribution of working group I to the fifth assessment report of the intergovernmental panel on climate change* (pp. 571–657). Cambridge, UK: Cambridge University Press. https://doi.org/10.1017/CBO9781107415324.016

Cai, W., Cowan, T., & Thatcher, M. (2012). Rainfall reductions over Southern Hemisphere semi-arid regions: The role of subtropical dry zone expansion. *Scientific Reports*, *2*, 702.

Caldeira, K., & Myhrvold, N. P. (2013). Projections of the pace of warming following an abrupt increase in atmospheric carbon dioxide concentration. *Environmental Research Letters*, *8*(3), 034039. https://doi.org/10.1088/1748-9326/8/3/034039

Davis, N., & Birner, T. (2017). On the discrepancies in tropical belt expansion between reanalyses and climate models and among tropical belt width metrics. *Journal of Climate*, *30*(4), 1211–1231.

Davis, S. M., & Rosenlof, K. H. (2012). A multidiagnostic interco mparison of tropical-width time series using reanalyses and satellite observations. *Journal of Climate*, *25*(4), 1061–1078.

Davis, N. A., Seidel, D. J., Birner, T., Davis, S. M., & Tilmes, S. (2016). Changes in the width of the tropical belt due to simple radiative forcing changes in the GeoMIP simulations. *Atmospheric Chemistry and Physics*, *16*(15), 10,083–10,095. https://doi.org/10.5194/acp-16-10083-2016

Forster, P. M., Richardson, T., Maycock, A. C., Smith, C. J., Samset, B. H., Myhre, G., et al. (2016). Recommendations for diagnosing effective radiative forcing from climate models for CMIP6. *Journal of Geophysical Research: Atmospheres*, *121*, 12,460–12,475. https://doi.org/10.1002/2016JD025320

Garfinkel, C. I., Waugh, D. W., & Polvani, L. M. (2015). Recent Hadley cell expansion: The role of internal atmospheric variability in reconciling modeled and observed trends. *Geophysical Research Letters*, *42*, 10,824–10,831. https://doi.org/10.1002/2015GL066942

Grassi, B., Redaelli, G., Canziani, P. O., & Visconti, G. (2012). Effects of the PDO phase on the tropical belt width. *Journal of Climate*, *25*(9), 3282–3290.

Grise, K. M., Davis, S. M., Simpson, I. R., Waugh, D. W., Fu, Q., Allen, R. J., et al. (2019). Recent tropical expansion: Natural variability or forced response? *Journal of Climate*, *32*(5), 1551–1571.

Grise, K. M., Davis, S. M., Staten, P. W., & Adam, O. (2018). Regional and seasonal characteristics of the recent expansion of the tropics. *Journal of Climate*, *31*(17), 6839–6856.

Grise, K. M., & Polvani, L. M. (2016). Is climate sensitivity related to dynamical sensitivity? *Journal of Geophysical Research: Atmospheres*, *121*, 5159–5176. https://doi.org/10.1002/2015JD024687

Hoesly, R. M., Smith, S. J., Feng, L., Klimont, Z., Janssens-Maenhout, G., Pitkanen, T., et al. (2018). Historical (1750–2014) anthropogenic emissions of reactive gases and aerosols from the community emissions data system (CEDS). *Geoscientific Model Development (Online)*, *11*(PNNL-SA-123932), 369–408.

Horinouchi, T., Matsumura, S., Ose, T., & Takayabu, Y. N. (2019). Jet-precipitation relation and future change of the Mei-Yu-Baiu rainband and subtropical jet in CMIP5 coupled GCM simulations. *Journal of Climate*, *32*(8), 2247–2259.

Hu, Y., & Fu, Q. (2007). Observed poleward expansion of the Hadley circulation since 1979. *Atmospheric Chemistry and Physics*, *7*(19), 5229–5236.

Hu, Y., Tao, L., & Liu, J. (2013). Poleward expansion of the Hadley circulation in CMIP5 simulations. *Advances in Atmospheric Sciences*, *30*(3), 790–795.

Johnson, B., Haywood, J., & Hawcroft, M. (2019). Are changes in atmospheric circulation important for black carbon aerosol impacts on clouds, precipitation and radiation? *Journal of Geophysical Research: Atmospheres*, *124*, 7930–7950. https://doi.org/10.1029/2019JD030568

Koch, D., Schulz, M., Kinne, S., McNaughton, C., Spackman, J. R., Balkanski, Y., et al. (2009). Evaluation of black carbon estimations in global aerosol models. *Atmospheric Chemistry and Physics*, *9*(22), 9001–9026.

Kovilakam, M., & Mahajan, S. (2015). Black carbon aerosol-induced Northern Hemisphere tropical expansion. *Geophysical Research Letters*, *42*, 4964–4972. https://doi.org/10.1002/2015GL064559

Liu, L., Shawki, D., Voulgarakis, A., Kasoar, M., Samset, B., Myhre, G., et al. (2018). A PDRMIP multimodel study on the impacts of regional aerosol forcings on global and regional precipitation. *Journal of Climate*, *31*(11), 4429–4447.

Lu, J., Chen, G., & Frierson, D. M. (2008). Response of the zonal mean atmospheric circulation to El Niño versus global warming. *Journal of Climate*, *21*(22), 5835–5851.

Lu, J., Vecchi, G. A., & Reichler, T. (2007). Expansion of the Hadley cell under global warming. *Geophysical Research Letters*, *34*, L06805. https://doi.org/10.1029/2006GL028443

Lucas, C., Timbal, B., & Nguyen, H. (2014). The expanding tropics: A critical assessment of the observational and modeling studies. *Wiley Interdisciplinary Reviews: Climate Change*, *5*(1), 89–112.

Mantsis, D. F., Sherwood, S., Allen, R., & Shi, L. (2017). Natural variations of tropical width and recent trends. *Geophysical Research Letters*, *44*, 3825–3832. https://doi.org/10.1002/2016GL072097

Min, S.-K., & Son, S.-W. (2013). Multimodel attribution of the Southern Hemisphere Hadley cell widening: Major role of ozone depletion. *Journal of Geophysical Research: Atmospheres*, *118*, 3007–3015. https://doi.org/10.1002/jgrd.50232

Myhre, G., Forster, P., Samset, B., Hodnebrog, Ø., Sillmann, J., Aalbergsjø, S., et al. (2017). Pdrmip: A precipitation driver and response model intercomparison projectñprotocol and preliminary results. *Bulletin of the American Meteorological Society*, *98*(6), 1185–1198.

Myhre, G., Shindell, D., Bréon, F., Collins, W., Fuglestvedt, J., Huang, J., et al. (2013). *Anthropogenic and natural radiative forcing, climate change 2013: The physical science basis. contribution of working group I to the fifth assessment report of the intergovernmental panel on climate change*, (pp. 659–740). Cambridge: Cambridge University Press.

Nguyen, H., Evans, A., Lucas, C., Smith, I., & Timbal, B. (2013). The Hadley circulation in reanalyses: Climatology, variability, and change. *Journal of Climate*, *26*(10), 3357–3376.

Polvani, L. M., Waugh, D. W., Correa, G. J., & Son, S.-W. (2011). Stratospheric ozone depletion: The main driver of twentieth-century atmospheric circulation changes in the Southern Hemisphere. *Journal of Climate*, *24*(3), 795–812.

Ramanathan, V., & Carmichael, G. (2008). Global and regional climate changes due to black carbon. *Nature Geoscience*, *1*, 221–227.

Rao, S., Klimont, Z., Smith, S. J., Van Dingenen, R., Dentener, F., Bouwman, L., et al. (2017). Future air pollution in the shared socio-economic pathways. *Global Environmental Change*, *42*, 346–358.

Samset, B., Myhre, G., Forster, P., Hodnebrog, Ø., Andrews, T., Faluvegi, G., et al. (2016). Fast and slow precipitation responses to individual climate forcers: A PDRMIP multimodel study. *Geophysical Research Letters*, *43*, 2782–2791. https://doi.org/10.1002/2016GL068064

Scheff, J., & Frierson, D. M. (2012). Robust future precipitation declines in CMIP5 largely reflect the poleward expansion of model subtropical dry zones. *Geophysical Research Letters*, *39*, L18704. https://doi.org/10.1029/2012GL052910

Schneider, T. (2006). The general circulation of the atmosphere. *Annual Review of Earth and Planetary Sciences*, *34*(1), 655–688. https://doi.org/10.1146/annurev.earth.34.031405.125144

Schwendike, J., Govekar, P., Reeder, M. J., Wardle, R., Berry, G. J., & Jakob, C. (2014). Local partitioning of the overturning circulation in the tropics and the connection to the Hadley and Walker circulations. *Journal of Geophysical Research: Atmospheres*, *119*, 1322–1339. https://doi.org/10.1002/2013JD020742

Seidel, D. J., Fu, Q., Randel, W. J., & Reichler, T. J. (2008). Widening of the tropical belt in a changing climate. *Nature Geoscience*, *1*(1), 21–24.

Shaw, T. A. (2014). On the role of planetary-scale waves in the abrupt seasonal transition of the Northern Hemisphere general circulation. *Journal of the Atmospheric Sciences*, *71*(5), 1724–1746. https://doi.org/10.1175/JAS-D-13-0137.1

Shaw, T. A., & Voigt, A. (2015). Tug of war on summertime circulation between radiative forcing and sea surface warming. *Nature Geoscience*, *8*(7), 560–566. https://doi.org/10.1038/ngeo2449

Shen, Z., & Ming, Y. (2018). The influence of aerosol absorption on the extratropical circulation. *Journal of Climate*, *31*(15), 5961–5975.

Sousa, P., Trigo, R., Aizpurua, P., Nieto, R., Gimeno, L., & Garcia-Herrera, R. (2011). Trends and extremes of drought indices throughout the 20th century in the Mediterranean. *Natural Hazards and Earth System Sciences*, *11*(1), 33–51.

Staten, P. W., Grise, K. M., Davis, S. M., Karnauskas, K., & Davis, N. (2019). Regional widening of tropical overturning: Forced change, natural variability, and recent trends. *Journal of Geophysical Research: Atmospheres*, *124*, 6104–6119. https://doi.org/10.1029/2018JD030100

Staten, P. W., Lu, J., Grise, K. M., Davis, S. M., & Birner, T. (2018). Re-examining tropical expansion. *Nature Climate Change*, *8*(9), 768–775.

Stjern, C. W., Samset, B. H., Myhre, G., Forster, P. M., Hodnebrog, Ø., Andrews, T., et al. (2017). Rapid adjustments cause weak surface temperature response to increased black carbon concentrations. *Journal of Geophysical Research: Atmospheres*, *122*, 11,462–11,481. https://doi.org/10.1002/2017JD027326

Tandon, N. F., Gerber, E. P., Sobel, A. H., & Polvani, L. M. (2013). Understanding Hadley cell expansion versus contraction: Insights from simplified models and implications for recent observations. *Journal of Climate*, *26*(12), 4304–4321.

Tang, T., Shindell, D., Samset, B. H., Boucher, O., Forster, P. M., Hodnebrog, Ø., et al. (2018). Dynamical response of Mediterranean precipitation to greenhouse gases and aerosols. *Atmospheric Chemistry and Physics*, *18*(11), 8439–8452. https://doi.org/10.5194/acp-18-8439-2018

Tao, L., Hu, Y., & Liu, J. (2016). Anthropogenic forcing on the Hadley circulation in CMIP5 simulations. *Climate Dynamics*, *46*(9-10), 3337–3350.

Watt-Meyer, O., Frierson, D., & Fu, Q. (2019). Hemispheric asymmetry of tropical expansion under $CO_2$ forcing. *Geophysical Research Letters*, *46*, 9231–9240. https://doi.org/10.1029/2019GL083695

Waugh, D. W., Garfinkel, C. I., & Polvani, L. M. (2015). Drivers of the recent tropical expansion in the Southern Hemisphere: Changing ssts or ozone depletion? *Journal of Climate*, *28*(16), 6581–6586.

Waugh, D. W., Grise, K. M., Seviour, W. J., Davis, S. M., Davis, N., Adam, O., et al. (2018). Revisiting the relationship among metrics of tropical expansion. *Journal of Climate*, *31*(18), 7565–7581.